Characterization of nanostructured bulk cobalt triantimonide doped with tellurium and indium prepared by pulsed plasma in liquid method

R. ZYBAŁA[1,2]*, M. SCHMIDT[2], K. KASZYCA[2], M. CHMIELEWSKI[2], M.J. KRUSZEWSKI[3], M. JASIŃSKI[4], M. RAJSKA[5], and Ł. CIUPIŃSKI[3]

[1] University Research Centre "Functional Materials", Warsaw University of Technology, 141 Wołoska St., 02-507 Warsaw, Poland;

[2] Łukasiewicz Research – Network Institute of Electronic Materials Technology, 133 Wólczyńska St., 01-919 Warsaw, Poland;

[3] Faculty of Materials Science and Engineering, Warsaw University of Technology, 141 Wołoska St., 02-507 Warsaw, Poland;

[4] Institute of Technology, Pedagogical University of Krakow, 2 Podchorążych St., 30-084 Krakow, Poland;

[5] Department of Inorganic Chemistry, Faculty of Materials Science and Ceramic, AGH University of Science and Technology, Krakow, 30 Mickiewicza Av., 30-059, Pola

Abstract. One of the ways to decrease thermal conductivity is nano structurization. Cobalt triantimonide ($CoSb_3$) samples with added indium or tellurium were prepared by the direct fusion technique from high purity elements. Ingots were pulverized and re-compacted to form electrodes. Then, the pulsed plasma in liquid (PPL) method was applied. All materials were consolidated using rapid spark plasma sintering (SPS). For the analysis, methods such as X-ray diffraction (XRD), scanning electron microscopy (SEM) and scanning transmission electron microscopy (STEM) with a laser flash apparatus (LFA) were used. For density measurement, the Archimedes' method was used. Electrical conductivity was measured using a standard four-wire method. The Seebeck coefficient was calculated to form measured Seebeck voltage in the sample placed in a temperature gradient. The preparation method allowed for obtaining $CoSb_3$ nanomaterial with significantly lower thermal conductivity ($10 \ Wm^{-1}K^{-1}$ for pure $CoSb_3$ and $3 \ Wm^{-1}K^{-1}$ for the nanostructured sample in room temperature (RT)). The size of crystallites (from SEM observations) in the powders prepared was about 20 nm, joined into larger agglomerates. The Seebeck coefficient, α, was about $-200 \ \mu VK^{-1}$ in the case of both dopants, In and Te, in microsized material and about $-400 \ \mu VK^{-1}$ for the nanomaterial at RT. For pure $CoSb_3$, α was about $150 \ \mu VK^{-1}$ and it stood at $-50 \ \mu VK^{-1}$ for nanomaterial at RT. In bulk nanomaterial samples, due to a decrease in electrical conductivity and inversion of the Seebeck coefficient, there was no increase in ZT values and the ZT for the nanosized material was below 0.02 in the measured temperature range, while for microsized In-doped sample it reached maximum ZT = 0.7 in (600K).

Key words: thermoelectric materials, nanostructured materials, skutterudite, energy harvesting, spark plasma sintering.

1. Introduction

Optimized thermoelectric (TE) materials can be used for direct energy conversion from heat into electricity in thermoelectric generators (TEG). The generators can be used for clean energy supply and waste heat energy harvesting. High-efficiency TEGs and TEMs (Thermoelectric Module – Peltier Module) may differ, especially in terms of material compositions, depending on the operational temperature. Generally, TEG modules should work with high-temperature gradients [1–3]. The efficiency of the conversion process in such a module depends on the Carnot cycle efficiency and material properties, described by the thermoelectric figure-of-merit (ZT). This ZT parameter merges electrical conductivity, σ, Seebeck coefficient, α, and thermal conductivity, λ. The thermoelectric figure of merit can be written as $ZT = \alpha^2 \cdot \sigma \cdot \lambda^{-1} \cdot T$, and it informs indirectly

about module efficiency [4]. To enhance this parameter, it is necessary to increase the Seebeck coefficient and electric conductivity and to reduce the thermal conductivity of the TE material.

Unfortunately, these material properties are interdependent [5]. Thus, a viable strategy for maximizing ZT may consist in first, minimizing lattice thermal conductivity, e.g. by material nano structurization that increases phonon scattering, and then by maximizing the power factor ($P_f = \alpha^2 \cdot \sigma$) through controlling chemical composition and optimum doping. For a wide range of applications, a bulk thermoelectric material with low lattice thermal conductivity and a high power factor is needed [6, 7]. To meet this need, modification of the material in the atomic, nano- and mesoscale [8–10] is necessary. A significant portion of phonons should be scattered on lattice imperfections and grain boundaries to decrease thermal conductivity. In the nanoscale, it is possible to tune thermoelectric properties by creating superlattices, quantum dots, nanowires and nanocomposites [11]. The work performed by Yu-Ming Lin et al. for Bi nanowires indicates that it is possible to obtain a very high ZT with wire dimensions between 10 and 5 nm [12].

R. Zybała, M. Schmidt, K. Kaszyca, M. Chmielewski, M.J. Kruszewski, M. Jasiński, M. Rajska, and Ł. Ciupiński

The anisotropy of the material can also be used to tune thermoelectric properties along the desired direction [13, 14].

CoSb$_3$ is a TE material from the skutterudite family that is known as a narrow band-gap semiconductor with a parabolic bottom of the conduction band. Optimally doped materials from these groups are state-of-the-art TE materials [15, 16]. For the purpose of this work, indium and tellurium dopants were chosen; these were reported earlier as ingredients that strongly increase the ZT values of CoSb$_3$ [17, 18]. The impact of the pulsed plasma in liquid (PPL) nano structurization process on the thermal properties of pure CoSb$_3$ was analyzed in our preliminary work [19] and shows that it is a possible route to strong reduction in thermal conductivity of the bulk nanomaterial being prepared.

In order to prepare nanosized powders, various methods, including laser ablation [20, 21], flame processing, vapor deposition, radio frequency and microwave plasma synthesis, plasma spray synthesis [22, 23], sol-gel processing and mechanical milling can be used [24, 25]. All of the above-mentioned methods have their weaknesses such as productive efficiency, costs or energy intensiveness. In this paper, we present state-of-the-art CoSb$_3$ [26, 27] thermoelectric material doped by In and Te obtained using PPL [28]. The prepared nanopowders were compacted by means of the solid state rapid consolidation spark plasma sintering (SPS) technique [29–31] to obtain bulk samples. The PPL method of powder preparation followed by rapid SPS densification could be a highly efficient manner to obtain bulk nanosized CoSb$_3$ thermoelectric material.

Electrical discharges observed in liquids are corona or corona-like discharges, pulsed arcs or sparks [32]. PPL with low energy discharge can be used to obtain metastable phases, nanoparticles, etc. because of short duration of the pulse discharge and the surrounding dielectric liquid providing fast cooling. A plasma pulse emerges between electrodes during short electrical breakdowns forced by a high electrical field. The energy generated can evaporate, melt and activate many types of materials of which the electrodes are made, concurrently enabling reaction with a liquid [33, 34], which can also create a protective layer on the particles [35–38]. Various types of nanomaterials can also be obtained by changing the liquid or electrodes [37, 39, 40]. The scheme of the system used in the present study is shown in Fig. 1, and it is similar to the apparatus employed by other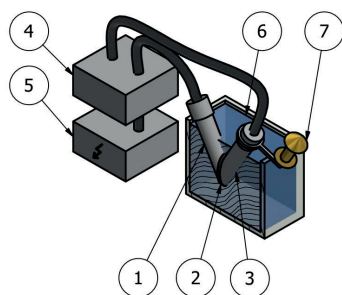s [34–36, 41, 42]. In our earlier work [43], we have presented preparation of nanoparticles of the CoSb$_3$ thermoelectric compound by means of the pulsed plasma in liquid (PPL) method. It was found that it is possible to obtain nanoparticles agglomerated in structures that have dimensions of about 1 μm, but from SEM observations it is clear that grains have diameters in the range of 10–30 nm. The XRD diffractograms for thus prepared PPL powders give smaller and more broadened signals, indicating the existence of nanograins or an amorphous phase.

Thermal conductivity was strongly decreased (more than two-fold) but the ZT parameter was very low and equal to about ~ 0.1 at the maximum point. The idea of this work was to check the influence on the ZT parameter by both reducing thermal conductivity with the use of nano structurization and by changing electrical properties by doping with tellurium and indium.

2. Materials and methods

2.1. Preparation of materials. For the synthesis, powdered high purity elements (99.99%) were used in amounts corresponding to the stoichiometric composition of the CoSb$_3$ compound. The substrates were mixed in a mechanical mortar grinder. The synthesis was performed in evacuated ($P_{vac} \approx 1 \times 10^{-3}$ mbar) tight quartz ampoules. It took place as a two-step process. First, the reagents were heated to 950°C, annealed for 60 minutes, followed by cooling the sample to ambient temperature. Then, the ingot was ground in an agate mortar and placed in a closed quartz ampoule. During the second stage, the ampoule with the powder was heated to 650°C, annealed for 7 days and cooled slowly [44]. After the synthesis, the material was milled again and the prepared powder was placed in a graphite die for the compaction process in the SPS apparatus under vacuum, at 50 MPa and 650°C to form dense electrodes of polycrystalline CoSb$_3$ [26]. The total time of the sintering process was approximately 30 minutes. Three series of samples were prepared for the experiments. The first one of pure CoSb$_3$, the second of CoSb$_3$ with indium (CoSb$_3$:In0.1), and the last one with tellurium (CoSb$_3$:Te0.1). 3 samples were prepared for each material (CoSb$_3$, CoSb$_3$+In, and CoSb$_3$+Te): 2 samples that were later used for the PPL process and one sample per every composition for measurements. A sample of PPL powders was also prepared for each material. It was later cut and used for electrical measurements ($\phi = 10$ mm, $h = 10$ mm).

2.2. PPL preparation of nanoparticles. In order to produce nanosized powder from the CoSb$_3$ electrodes, the PPL method was used. Two polycrystalline CoSb$_3$ electrodes were placed in an isopropyl alcohol bath at a pre-defined separation distance. Next, 320 V DC was applied to the system. Additionally, an electrode distance regulator was activated to provide vibration and control the distance within the range of 0–0.3 mm. The maximum energy of a single discharge during the process was below 45 mJ. The powder yield was ~ 0.25 g/h. For the electrical and thermal measurements, the nanosized powders after the PPL process were sintered into bulk samples again ($\phi = 10$ mm, $h = 10$ mm). The sintering parameters for the

Fig. 1. Pulsed plasma in liquid system scheme: 1, 3 – CoSb$_3$ electrodes, 2 – pulsed plasma, 4 – discharge controller, 5 – power supply, 6 – isopropyl alcohol, 7 – vibrator with electrode distance regulator

Characterization of nanostructured bulk cobalt triantimonide doped with tellurium and indium prepared by pulsed plasma in liquid method

nanosized powders were similar to that used for the microsized material. The sintering time for the PPL materials was shorter, to avoid grain growth, and equaled 5 min.

2.3. Metallographic section preparations. The metallographic section for the SEM observation was prepared by polishing the diamond paste. To enhance visibility of grain boundaries, the etching agent, with composition of 10 g tartaric acid ($C_4H_6O_6$), 15 cm^3 nitric acid (HNO_3) and 90 cm^3 of deionized water, was used. The time of the etching agent treatment was approximately 10 min.

2.4. Characterization of materials microstructure. The structural and microstructural analyses of the powders and sinters at every step of the experiment were performed using an X-ray diffractometer (Bruker D8 Advance) and scanning electron microscope (Hitachi SU8000). The microstructure of the sintered fine-grained $CoSb_3$ materials was characterized by means of X-ray diffraction (XRD), scanning electron microscopy (SEM) and scanning transmission electron microscopy (STEM) (Hitachi HD 2700, 200 kV, Cs-corrected). The grain size distribution of the powder was measured using an LA-950 HORIBA laser-scattering particle size distribution analyzer.

2.5. Electrical measurements. The electrical conductivity and the Seebeck coefficient of all of the samples were measured using specially design apparatus (SeebTest apparatus from PESS). The idea behind the method is presented in Fig. 2. The Seebeck coefficient was calculated from the Seebeck voltage measurement after temperature stabilization. First without temperature gradient (T1 = T2) and then in the temperature gradient equal to about 5 K. The thermocouple shields (isolated from the thermoelement) act as electrodes. The measurements errors were estimated based on the standard deviation of the measured electrical and temperature data.
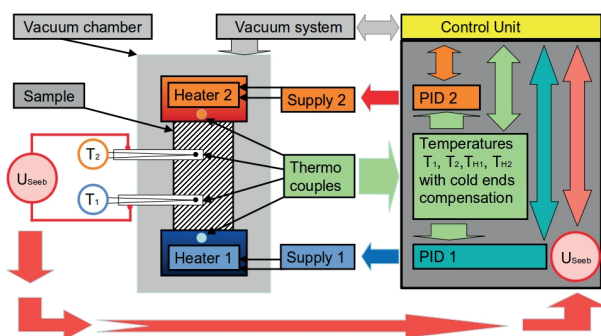

Fig. 2. Scheme of the apparatus for electrical measurements (SeebTest)

Electrical conductivity measurements took place in the same apparatus when T1 = T2 with heater thermocouples acting as electrodes. 2,000 points were collected during a single temperature point measurement, and polarization of the current was changed after every 200 measurements. The electric current was stabilized and equal to about 500 mA. Measurements errors were calculated from the measurements.

All measurements took place under low pressure (10 mBar) with argon as the atmosphere. The apparatus can be used in the range of temperatures, from room temperature to 500°C (if corrosion of the sample does not occur). All parameters are controlled and analyzed by specialized software. Cold ends of thermocouples and additionally Seebeck voltages measured on the reference samples are included in the compensation. Repeatability is very good and it is within the measurement error range. All measurements were made under stationary conditions. One series of measurements took about 2 days for one sample.
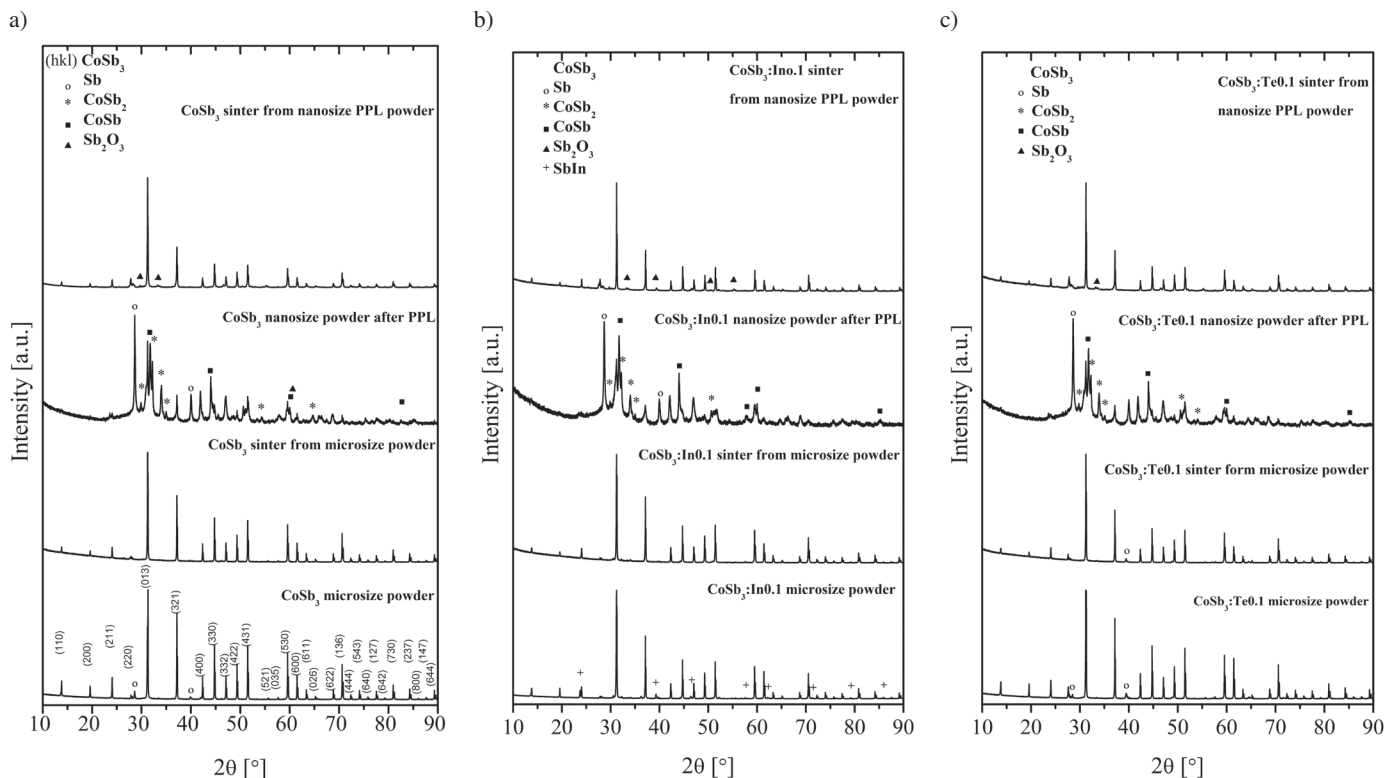
The errors of electrical measurement (Seebeck coefficient and electrical conductivity) were very notable and they stood below 10% with repeatability below 3%. The errors for LFA measurements of thermal conductivity were below 5% with repeatability at 1%. ZT errors were calculated from partial derivatives and in our experiments amounted to about 5%. These calculations were based on measurement errors. Although, when we take maximum errors of the methods into account, the errors of the ZT parameter can reach even 30%.

2.6. Thermal conductivity. Thermal conductivity was determined for both the microstructural and nanostructural materials, using the laser flash method (LFA 457-Netzsch) [45]. For the LFA measurements, a sample with the dimensions of $\phi = 10$ mm and $h = 2$ mm was prepared. The densities for calculations were measured by the Archimedes' method with water as the liquid. The thermal capacities of the samples were established by the comparative method involving the reference sample.

3. Results

3.1. XRD. The XRD diffraction patterns for the $CoSb_3$ primary powders and sinters, used later as electrodes (microsized), show visible differences in comparison to the powders prepared by the PPL method (nanosized) and their sinters in Fig. 3.

The microsized powder exhibits strong peaks from the $CoSb_3$ phase, with a weak signal from pure Sb. Similar diffraction patterns, but without a reflection from Sb, were obtained from the sample after the sintering process. The powder prepared by the PPL method shows a significantly different XRD pattern, with faint reflections from the $CoSb_3$ phase and strong background indicating a high percentage of nanosized and amorphous material. Additionally, peaks from other phases, such as $CoSb_2$, $CoSb$, and Sb, have comparable intensity. The bulk material prepared from the PPL powder is characterized by reappearance of strong reflections from crystallites, which were attributed to grain size growth during the sintering process and reactions occurring between impurities. There is also a small amount of another phase, namely Sb_2O_3, and phases like $CoSb_2$ and Sb, already identified for the electrode material, are present in lower quantities. Diffraction patterns for $CoSb_3$ with In or Te exhibit similar tendencies. In the case of In, the starting material has InSb impurities, which later vanish, leaving only a pure $CoSb_3$ phase with a small amount of Sb_2O_3.

R. Zybała, M. Schmidt, K. Kaszyca, M. Chmielewski, M.J. Kruszewski, M. Jasiński, M. Rajska, and Ł. Ciupiński

Fig. 3. XRD patterns for: a) $CoSb_3$, b) $CoSb_3$:In0.1, c) $CoSb_3$:Te0.1

In the material with Te, there is only a pure $CoSb_3$ phase and some Sb_2O_3 impurities. The lattice parameter for each sample, as estimated by the Rietveld refinement method from the XRD pattern, is presented in Table 1. The lattice parameters are a little higher for the material following the PPL process. The lattice parameters for pure $CoSb_3$ and $CoSb_3$:Te0.1 are higher than those observed by Liu et al. [17].

Table 1: Estimated lattice parameters from XRD patterns

Material		Lattice parameter [Å]
$CoSb_3$	Synthesized	9.048 ± 0.001
	After PPL	9.050 ± 0.001
$CoSb_3$:In0.1	Synthesized	9.060 ± 0.001
	After PPL	9.073 ± 0.001
$CoSb_3$:Te0.1	Synthesized	9.054 ± 0.001
	After PPL	9.065 ± 0.001

3.2. SEM/STEM/particle size distribution. The SEM image in Fig. 4a shows the $CoSb_3$ microsized powder with sharp edges and irregular shapes. Representative STEM (SE – secondary electron) images of the PPL powder show the formation of agglomerates composed of nanosized spheroidal particles (Fig. 4b), creating a spatial structure. The particle size distribution can be seen in Fig. 4c. For the primary $CoSb_3$ powder,

the median size of the particles is 4 μm and the mean size is 5 μm. For the PPL powder, the median size is 0.79 μm and the mean size is 1.0 μm. For the second series of samples, the morphology is similar. The primary $CoSb_3$:In0.1 powder (Fig. 4d–f) shows the median particles size of 2.6 μm and the mean size is 4 μm. For the PPL powder, the median size is 1.2 μm and the
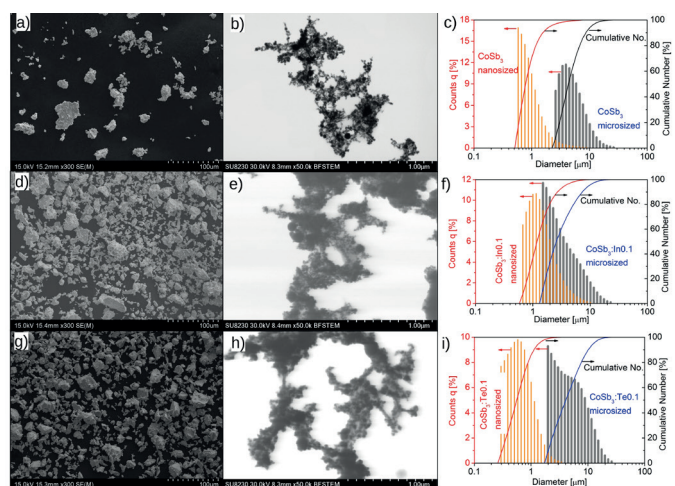

Fig. 4. SEM image of: a) $CoSb_3$ powder, b) STEM nanosized PPL $CoSb_3$ powder, c) particle size distribution. SEM image of d) $CoSb_3$:In0.1 powder, e) STEM nanosized PPL $CoSb_3$:In0.1 powder, f) particle size distribution. SEM image of: g) $CoSb_3$:Te0.1 powder, h) STEM nanosized PPL $CoSb_3$:Te0.1 powder, i) particle size distribution

www.czasopisma.pan.pl   PAN   www.journals.pan.pl
POLSKA AKADEMIA NAUK

Characterization of nanostructured bulk cobalt triantimonide doped with tellurium and indium prepared by pulsed plasma in liquid method

mean size is 2 μm. Similar morphology was also observed for the third series of samples. The primary $CoSb_3$:Te0.1 powder (Fig. 4g–i) has a median particle size of 4.1 μm, and a mean size of 6 μm. For the PPL powder, the median size is 0.56 μm and the mean size is 0.7 μm. The data were collected and presented in Table 2.

Table 2: Measured parameters for particle size distribution

Material		d_{mean} [μm]	d_{10} [μm]	d_{90} [μm]	d_{med} [μm]
$CoSb_3$	Synthesized	5 ± 3	2.66	8.65	4.32
	After PPL	1.0 ± 0.7	0.55	1.57	0.79
$CoSb_3$:In0.1	Synthesized	4 ± 3	1.48	7.30	2.57
	After PPL	2 ± 1	0.69	2.70	1.18
$CoSb_3$:Te0.1	Synthesized	6 ± 3	2.00	10.14	4.07
	After PPL	0.7 ± 0.3	0.31	1.13	0.56

It should be noted here that, based on the microstructural observation (STEM), the estimated individual grain size of PPL powders is much lower (about 20 nm) and this population dominates in the agglomerates structure. The particle size results and the STEM observation-estimated size discrepancy is due to the conditions of the PPL process because of the process where small crystallites are forming agglomerates during rapid cooling of the evaporated material.

In Fig. 5, we can see the SEM images for the metallographic section of the sinters. For materials prepared from microsized powders, shown in Fig. 5, the diameters of the crystallites are within the range of 10 to 20 μm.
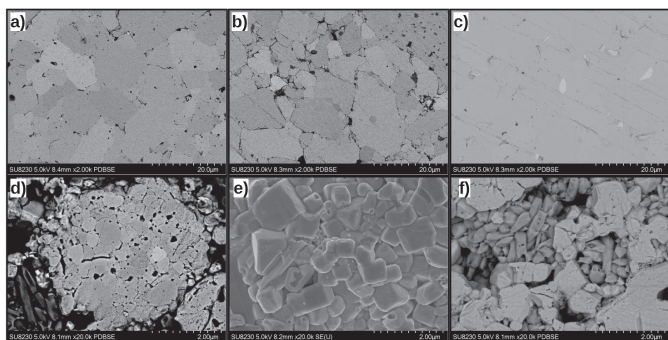

Fig. 5. SEM images of metallographic section of sinters: a) $CoSb_3$ microsized, b) $CoSb_3$:In0.1 microsized, c) $CoSb_3$:Te0.1 microsized and d) $CoSb_3$ PPL, e) $CoSb_3$:In0.1 PPL, f) $CoSb_3$:Te0.1 PPL

For materials sintered from powders prepared by the PPL technique (Fig. 5d–f), the grain diameter is more than one order of magnitude smaller than in the previous cases and the average crystallite size is in the order of nanometers. The visible porosity may be an effect of mechanical polishing and the chemical treatment but also may be due to the sintering conditions. The densities of all samples measured by the Archimedes' method

in water for microsized and nanosized material and compared with crystallographic value are presented in Table 3.

Table 3: Samples densities

Material		Measurement, density [g/cm^3]	From XRD, density [g/cm^3]
$CoSb_3$	Synthesized	7.66 ± 0.05	7.61 ± 0.01
	After PPL	6.49 ± 0.01	7.60 ± 0.01
$CoSb_3$:In0.1	Synthesized	7.69 ± 0.04	7.58 ± 0.01 (In in cages)
	After PPL	6.34 ± 0.05	7.55 ± 0.01 (In in cages)
$CoSb_3$:Te0.1	Synthesized	7.64 ± 0.03	7.38 ± 0.01 (Te in Sb places)
	After PPL	6.58 ± 0.04	7.35 ± 0.01 (Te in Sb places)

3.3. Electrical properties. The Seebeck coefficient and electrical conductivity are presented in Fig. 6a. The Seebeck coefficient is positive and in the range of 120–175 μVK^{-1} for pure
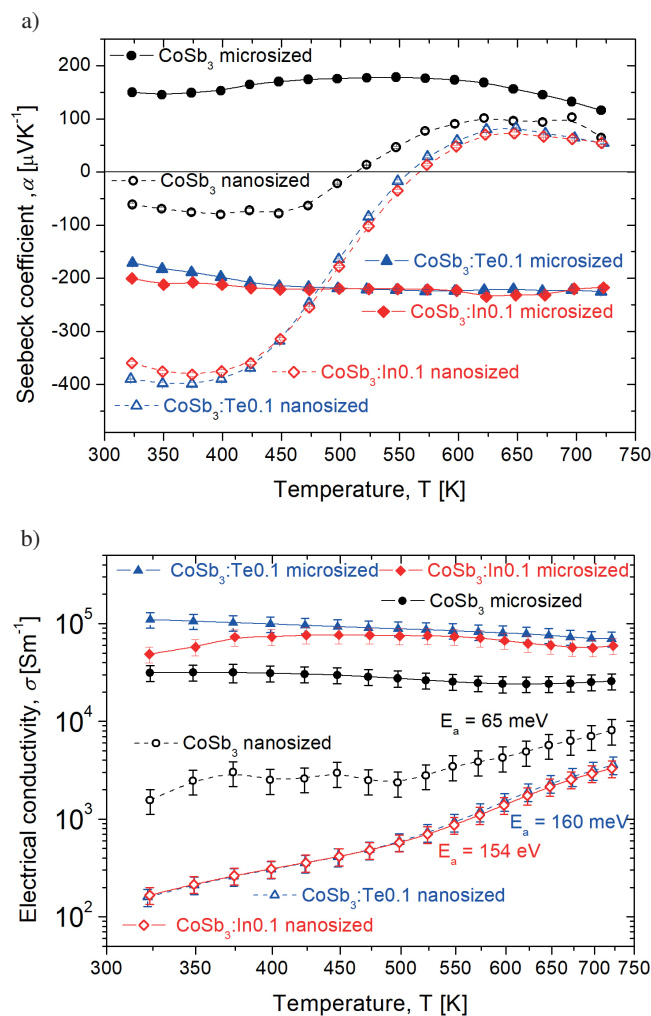

Fig. 6. Temperature dependencies of: a) Seebeck coefficient; b) electrical conductivity for sinters with nano and microstructures

CoSb$_3$, which is a value similar to that obtained by other researchers employing a similar preparation method [45].

The Seebeck coefficient for CoSb$_3$ PPL materials is in the range of -75 to $100~\mu\text{VK}^{-1}$ and alters its sign with temperature, negative below 550 K and positive for higher temperatures.

A similar tendency in the Seebeck coefficient for pure CoSb$_3$ was observed by other researchers [26, 46].

For the microsized materials doped with In and Te, the Seebeck coefficient possesses negative values in the range of 225–170 μVK^{-1}. For the PPL-doped materials, the Seebeck coefficient changes from high negative values, i.e. $-400~\mu\text{VK}^{-1}$, going through 0 at 550 K and reaching 80 μVK^{-1} at higher temperatures. For all of the PPL materials, the Seebeck coefficient has an "S" shaped temperature dependency curve. The measurement errors were negligible and are not presented in the graphs. The error values were in the range of 1–6 μVK^{-1} for all measured samples.

The electrical conductivity (Fig. 6b) for microsized material decreases with temperature, exhibiting metallic properties. However, the sample sintered from the PPL powders shows a different behavior. Electrical conductivity is lower by two orders of magnitude and increases with temperature, thus indicating semiconducting properties. The estimated activation energy of electrical conductivity, Ea, for PPL In and Te in all temperature ranges is equal to 154 and 160 meV, respectively. The PPL CoSb$_3$ possesses an activating character of electrical conductivity at higher temperatures.

3.4. Thermal properties. In Fig. 7 values of thermal conductivity and the electronic parts of thermal conductivity calculated from measured values of electrical conductivity are presented. For the LFA method, total thermal conductivity was calculated using the equation $\lambda_{\text{tot}} = C_p \cdot \rho \cdot \alpha$, where: C_p is specific heat, ρ is density, and α is thermal diffusivity [47]. The electronic part of thermal conductivity was calculated from the Wiedemann-Franz law equation, i.e. $\lambda_{el} = L \cdot \sigma \cdot T$. The values of electrical conductivity, densities and thermal diffusivity for this were measured by a comparative method using LFA apparatus; for calculations, the L parameter, $2.44 \times 10^{-8}\text{W}\Omega\text{K}^{-2}$, was taken from the literature [45].

The data indicate that the fine-grained material prepared from the PPL powder exhibits thermal conductivity almost two-times lower than the coarse grain electrode material in the examined temperature range. At room temperature, thermal conductivity equals 3 Wm^{-1}K^{-1} for the PPL sinter and almost 10 Wm^{-1}K^{-1} for the electrode one. In both cases, thermal conductivity decreases with temperature and at 675 K is about 2 Wm^{-1}K^{-1} for the PPL sinter and 5 Wm^{-1}K^{-1} for the starting CoSb$_3$ material. The sharp decrease in thermal conductivity for the PPL sinter was attributed to the microstructure of the sinter with small grain size and increased volume fraction of grain boundaries. Another factor contributing to thermal conductivity is the observed decrease in electrical conductivity. The electronic part of thermal conductivity is much smaller for the PPL material and equals up to 0.15 Wm^{-1}K^{-1}, while the microsized material is up to 1.23 Wm^{-1}K^{-1}.
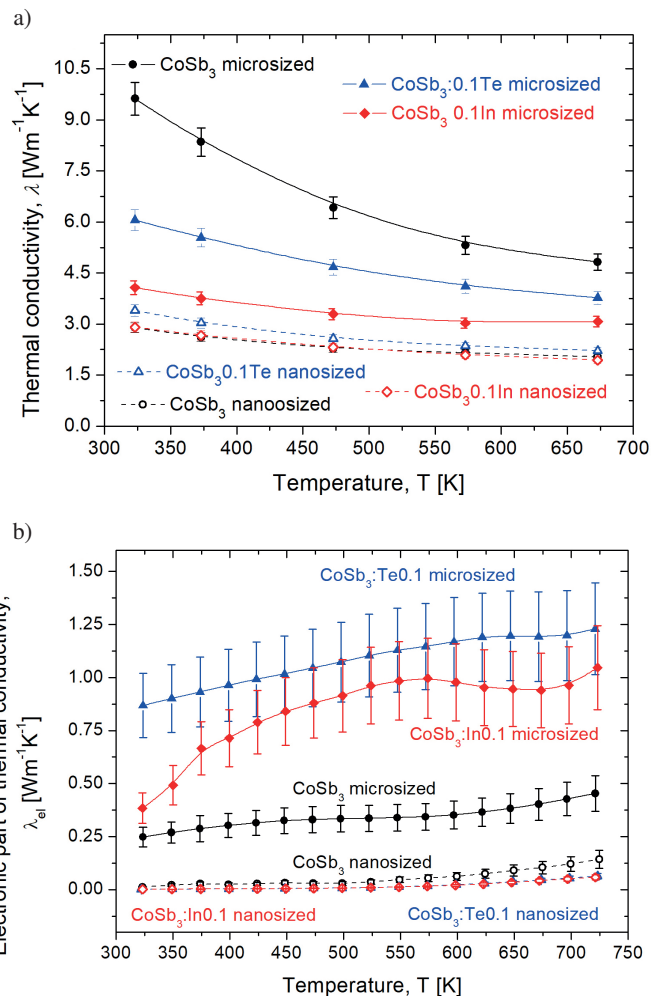
a)

b)

Fig. 7. Temperature dependencies of: a) thermal conductivity of all samples, and b) the electronic part of thermal conductivity

3.5. ZT parameter. The ZT parameter (Fig. 8) for CoSb$_3$ and the doped microsize material increases with temperature up to 600 K and then decreases. The highest value of ZT, 0.7, was
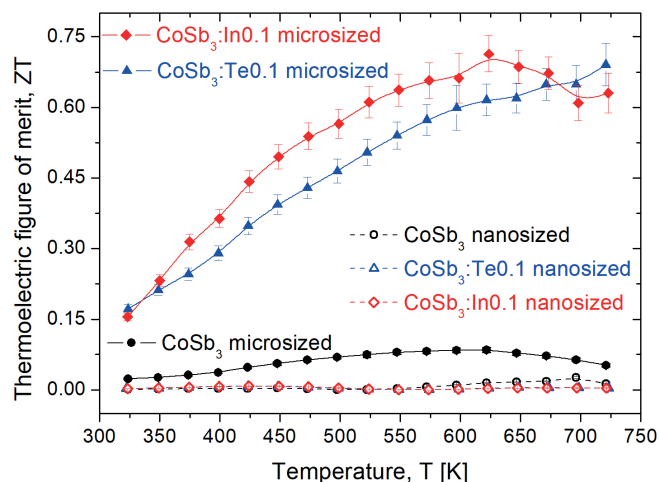

Fig. 8. Temperature dependency of ZT parameter for sinters with nano and microstructure

reached for the In-doped material at 625 K. Unfortunately, for the nanosized samples, the ZT parameter is much lower than for the microsized material, due to the sign inversion of the Seebeck coefficient at 550 K, and it is below 0.02 for all nanosized material.

4. Discussion

XRD measurements were taken at every step of the preparation. All of the sinters have strong peaks from the $CoSb_3$ phase, although for the powders after the PPL, due to the small grain size, the peaks are smaller and more broadened. Also, other phase signals, like $CoSb_2$ and $CoSb$, vanished after sintering. Some impurities in the last step could be eliminated by adjusting conditions and using better process control with the appropriate liquid which should be selected in future work. It is noteworthy that in all samples oxidation was negligible except for a small amount of Sb_2O_3 in the samples after sintering the nanopowders. The cell parameter increases after the PPL process and after addition of the dopant. The cell parameters of PPL powders are higher than in the In-doped $CoSb_3$ [49] or in the Te-doped material [18].

The SEM observations indicate that in all cases of PPL treatment a nanomaterial was obtained. The nanoparticles, after the PPL process, form larger agglomerates. The agglomerate diameters are presented in particle size distribution, and they are distinctly larger than the single PPL crystallite, however, they are still smaller than the crystallites in the starting powder. After the sintering process, there is visible growth of crystallites and for the microsized material used as electrode materials, the average diameter is 10 to 20 μm. For the sinters from the nano PPL powders, the average diameters for all the samples are comparable and about one order of magnitude smaller than the crystallites in the reference material. The densities of all the sinters from the microsized powders reach 100% of theoretical value. Unfortunately, the sinters from the nanosized powders prepared by the PPL method reach, in all cases, about 85% of theoretical value. This may be related to the sintering process because to avoid grain size growth, the sintering time was intentionally decreased from 15 to 5 min. Based on this experiment, the sintering condition should be adjusted to ensure higher PPL sample densification.

The Seebeck coefficient is positive and in the range of 120–175 μVK^{-1} for pure $CoSb_3$, which is a value similar to that obtained by other researchers employing a similar preparation process [45]. The positive sign of the Seebeck coefficient is also connected with the use of high purity elements for the synthesis. The Seebeck coefficient for the $CoSb_3$ PPL materials is in the range of -75 to 100 μVK^{-1} and alters its sign with temperature, negative below 550 K and positive for higher temperatures. Some researchers have noticed a similar tendency in the Seebeck coefficient for pure $CoSb_3$ [26, 46]. At low temperatures, Seebeck coefficients have high n-type absolute values, corresponding to the extrinsic region. When the conduction by minority carriers increases, the Seebeck coefficient decreases and becomes p-type for the lightly doped samples [26]. Also, it

is known that the Co-rich $CoSb_3$ phase acts as an n-type material while Sb acts as p-type [10], and the changes in concentration and mobility of the majority of carriers can lead to a change in the Seebeck coefficient sign from n-type to p-type. For all of the PPL materials, the Seebeck coefficient has an "S" shape for the temperature dependency curve. This may be explained, as in the case of $CoSb_3$, by the increase of the role of the intrinsic region. The phenomenon may also be related to changes in compositions and the Sb losses during the PPL process.

Electrical conductivity of all microsized materials exhibits metallic properties and decreases with temperature; whereas for the nanosized material, electrical conductivity increases with temperature and is almost one or two orders of magnitude lower than for the starting material. The electrical conductivity of the microsized In and Te-doped material is comparable with literature values [50, 51]. The nanosized PPL material has an activation character of electrical conductivity. It may be related to changes of the stoichiometry of the compound during the PPL process and dopant or Sb losses. Additionally, the lower density of the PPL sinters may be responsible for decreasing electrical conductivity.

At room temperature, thermal conductivity reaches 3 $Wm^{-1}K^{-1}$ for the PPL $CoSb_3$ sinter and almost 10 $Wm^{-1}K^{-1}$ for the microsized bulk material. In both cases, thermal conductivity decreases with temperature. The highest improvement was achieved for pure $CoSb_3$. Improvement of materials doped with In and Te was smaller because the starting material is characterized by conductivity lower than pure $CoSb_3$ and, at room temperature, it was equal to about 4 and 5 $Wm^{-1}K^{-1}$, respectively. All of the nanosized material has thermal conductivity of about 3–3.5 $Wm^{-1}K^{-1}$ at room temperature and its value is about 3 times lower than for pure $CoSb_3$. The data from the particle size distributions are correlated with thermal conductivity. For the material with Te, there is higher improvement in thermal conductivity than for the material with In. This improvement may be attributed to the microstructure of the sinter with small grain size and increased volume fraction of the grain boundaries. Another factor contributing to thermal conductivity is the observed decrease in electrical conductivity. The electronic part of thermal conductivity is much smaller for the PPL material and equals up to 0.15 $Wm^{-1}K^{-1}$ while for the microsized material this value reaches up to 1.23 $Wm^{-1}K^{-1}$ and it is related to changes from metallic to semiconducting properties of the samples after the PPL process. Because of the nano structurization process, presented in our work, significant improvement in decreasing thermal conductivity was achieved. This improvement is in agreement with Xie et al.'s work [52] that claims that nano structurization can improve the thermal properties of TE materials. Another factor responsible for lower thermal conductivity relates to the lower density of the PPL sinters, which reach about 85% of theoretical value, whereas for the microsize material densities they reach 100%.

For the material doped with In, the maximum ZT of 0.7 at 600 K is comparable with the ZT of 0.67 reported for $In_{0.35}Co_4Sb_{12}$ at 600 K [53]. The highest value of ZT, 0.7, was achieved for the microsized Te-doped material at 725 K, which

is comparable with Deng et al.'s work: ZT = 0.69 at 710 K [18]. Unfortunately, for the nanomaterials there was no improvement in the ZT parameter because the PPL bulk material has significantly lower electrical conductivity and the Seebeck coefficient changed its sign in the middle of the temperature range, thus resulting in a low ZT value.

It is possible that the introduction of defects like grain boundaries may influence dopant segregation, so the amount of dopant must be considered to improve thermoelectric properties. In this study, the Seebeck coefficient has the most negative impact on the ZT value. Some additional information from Hall measurements could prove helpful for understanding the changes in electrical properties after the preparation of the material by the PPL method.

5. Conclusions

A new approach to fabricating nanosized $CoSb_3$ TE material was used. The preparation of this state-of-the-art TE material from the skutterudite family, with the use of PPL with low-energy spark discharge, was presented. The PPL technique required the presence of dense electrodes made of single phase $CoSb_3$ material synthesized by a traditional synthesis method. The PPL preparation method enabled the obtaining of nanocrystalline $CoSb_3$ powders with grain size of 10–30 nm. After SPS, these powders were processed into bulk thermoelectric materials. Their thermal conductivity is over two times lower than for the microcrystalline materials. Reducing thermal conductivity in pure $CoSb_3$ and in the material doped with In and Te is very promising. Unfortunately, there was no improvement in the ZT parameter, because the PPL bulk material had significantly lower electrical conductivity and the Seebeck coefficient changed its sign in the middle of the temperature range, thus resulting in a low ZT value. For improvement of these nanomaterials in the future, optimization of the sintering process to increase density is needed along with adjustment of dopant concentration to increase the Seebeck coefficient and electrical conductivity, and thereby the ZT parameter.

REFERENCES

[1] R. Zybała, M. Schmidt, K. Kaszyca, Ł. Ciupiński, M.J. Kruszewski, and K. Pietrzak, "Method and apparatus for determining operational parameters of thermoelectric modules", *J. Electron. Mater*. 45 (10), 5223–5231 (2016).

[2] F.P. Brito, L. Figueiredo, L.A. Rocha, A.P. Cruz, L.M. Gonçalves, J. Martins and M.J. Hall, "Analysis of the effect of module thickness reduction on thermoelectric generator output", *J. Electron. Mater*. 45 (3), 1711–1729 (2016).

[3] K.T. Wojciechowski, R. Zybala, J. Leszczynski, P. Nieroda, M. Schmidt, R. Gajerski and E. Aleksandrova, "Performance characterization of high-efficiency segmented Bi 2Te3/CoSb3 unicouples for thermoelectric generators", *AIP Conf. Proc*. 1449 (1), 467–470 (2012).

[4] G.J. Snyder and E.S. Toberer, "Complex thermoelectric materials", *Nat. Mater*. 7 (2), 105–114 (2008).

[5] A.J. Minnich, M.S. Dresselhaus, Z.F. Ren, and G. Chen, "Bulk nanostructured thermoelectric materials: Current research and future prospects", *Energy Environ. Sci*. 2 (5), 466–479 (2009).

[6] P. Wen, B. Duan, P. Zhai, P. Li, and Q. Zhang, "Effect of thermal annealing on the microstructure and thermoelectric properties of nano-TiN/Co4Sb11.5Te0.5 composites", *J. Mater. Sci. Mater. Electron*. 24 (12), 5155–5161 (2013).

[7] Ł. Ciupiński, M.J. Kruszewski, J. Grzonka, M. Chmielewski, R. Zielińsk, D. Moszczyńska and A. Michalski, "Design of interfacial Cr3C2 carbide layer via optimization of sintering parameters used to fabricate copper/diamond composites for thermal management applications", *Mater. Des*. 120, 170–185 (2017).

[8] M.S. Dresselhaus, G. Dresselhaus, X. Sun, Z. Zhang, S.B. Cronin, and T. Koga, "Low-dimensional thermoelectric materials", *Phys. Solid State* 41 (5), 679–682 (1999).

[9] Z.G. Chen, G. Hana, L. Yanga, L. Cheng, and J. Zou, "Nanostructured thermoelectric materials: Current research and future challenge", *Progress in Natural Science: Materials International* 22 (6), 535–549 (2012).

[10] C. Gayner and K.K. Kar, "Recent advances in thermoelectric materials", *Progress in Materials Science* 83, Elsevier Ltd, 330–382 (2016).

[11] K. Biswas, J. He, I.D. Blum, C.I. Wu, T.P. Hogan, D.N. Seidman, V.P. Dravid and M.G. Kanatzidis, "High-performance bulk thermoelectrics with all-scale hierarchical architectures", *Nature* 489 (7416), 414–418 (2012).

[12] Y. Lin, X. Sun, and M.S. Dresselhaus, "Theoretical investigation of thermoelectric transport properties of cylindrical Bi nanowires", *Physical Review B* 62 (7), 4610–4623 (2000).

[13] R. Zybala and K.T. Wojciechowski, "Anisotropy analysis of thermoelectric properties of $Bi_2Te_{2.9}Se_{0.1}$ prepared by SPS method", in *AIP Conference Proceedings* 1449, 393–396 (2012).

[14] R. Zybała, K. Mars, A. Mikuła, J. Bogusławski, G. Soboń, J. Sotor, M. Schmidt, K. Kaszyca, M. Chmielewski, L. Ciupiński and K. Pietrzak, "Synthesis and Characterization of Antimony Telluride for Thermoelectric and Optoelectronic Applications", *Arch. Metall. Mater*. 62 (2), 1067–1070 (2017).

[15] S. Ballikaya, N. Uzar, S. Yildirim, J.R. Salvador, and C. Uher, "High thermoelectric performance of In, Yb, Ce multiple filled CoSb3based skutterudite compounds", *J. Solid State Chem*. 193, 31–35 (2012).

[16] J. Dong, K. Yang, B. Xu, L. Zhang, Q. Zhang, and Y. Tian, "Structure and thermoelectric properties of Se- and Se/Te-doped CoSb3 skutterudites synthesized by high-pressure technique", *J. Alloys Compd*. 647, 295–302 (2015).

[17] W.-S. Liu, B.-P. Zhang, J.-F. Li, H.-L. Zhang, and L.-D. Zhao, "Enhanced thermoelectric properties in CoSb3-xTex alloys prepared by mechanical alloying and spark plasma sintering", *J. Appl. Phys*. 102 (10), p. 103717 (2007).

www.czasopisma.pan.pl   PAN   www.journals.pan.pl
POLSKA AKADEMIA NAUK

Characterization of nanostructured bulk cobalt triantimonide doped with tellurium and indium prepared by pulsed plasma in liquid method

[18] L. Deng, H.A. Ma, T.C. Su, F.R. Yu, Y.J. Tian, Y.P. Jiang, N. Dong, S.Z. Zheng and X. Jia, "Enhanced thermoelectric properties in $Co_4Sb_{12-x}Te_x$ alloys prepared by HPHT", *Mater. Lett.* 63 (24–25), 2139–2141 (2009).

[19] R. Zybała, M. Schmidt, P. Kamińska, M.J. Kruszewski, J. Grzonka, K. Pietrzak and Ł. Ciupiński, "Skutterudite (CoSb3) thermoelectric nanomaterials fabricated by Pulse Plasma in Liquid", *Mater. Today Proc.* 5 (4), 10316–10322 (2018).

[20] V. Kosalathip, A. Dauscher, B. Lenoir, S. Migot, and T. Kumpeerapun, "Preparation of conventional thermoelectric nanopowders by pulsed laser fracture in water: Application to the fabrication of a pn hetero-junction", *Appl. Phys. A Mater. Sci. Process.* 93 (1), 235–240 (2008).

[21] J. Kusinski, S. Kac, A. Kopia, A. Radziszewska, M. Rozmus-Górnikowska, B. Major, L. Major, J. Marczak and A. Lisiecki, "Laser modification of the materials surface layer-a review paper", *Bull. Pol. Ac.: Tech.* 60 (4), 711–728 (2012).

[22] D. Szabó and S. Schlabach, "Microwave Plasma Synthesis of Materials – From Physics and Chemistry to Nanoparticles: A Materials Scientist's Viewpoint", *Inorganics* 2 (3), 468–507 (2014).

[23] X.-K. Huynh, B.-W. Kim and J.-S. Kim, "Fabrication of Fe-TiB2 Nanocomposites by Spark-Plasma Sintering of a (FeB, TiH2) Powder Mixture", *Arch. Metall. Mater.* 63 (2), 1043–1047 (2018).

[24] X. Chen, L. Liu, Y. Dong, L. Wang, L. Chen, and W. Jiang, "Preparation of nano-sized Bi_2Te_3 thermoelectric material powders by cryogenic grinding", *Prog. Nat. Sci. Mater. Int.* 22 (3), 201–206 (2012).

[25] K. Zaharieva, G. Vissokov, J. Grabis, and S. Rakovsky, "Plasma-chemical synthesis of nanosized powders-nitrides, carbides, oxides, carbon nanotubes and fullerenes", *Plasma Sci. Technol.* 14 (11), 980–995 (2012).

[26] M.J. Kruszewski, R. Zybała, Ł. Ciupiński, M. Chmielewski, B. Adamczyk-Cieślak, A. Michalski, M. Rajska and K.J. Kurzydłowski, "Microstructure and Thermoelectric Properties of Bulk Cobalt Antimonide ($CoSb_3$) Skutterudites Obtained by Pulse Plasma Sintering", *J. Electron. Mater.* 45 (3), 1369–1376 (2016).

[27] Y. Liu, X. Li, Q. Zhang, L. Zhang, D. Yu, B. Xu and Y. Tian, "High Pressure Synthesis of p-Type", *Materials (Basel).* 9 (4), p. 257 (2016).

[28] S. Sulaimankulova, E. Omurzak, J. Jasnakunov, A. Abdykerimova, H. Gafforova, and A. Mametova, "New preparation method of nanocrystalline materials by impulse plasma in liquid", *J. Clust. Sci.* 20 (1), 37–49 (2009).

[29] M. Singh, M. Miyata, S. Nishino, D. Mott, M. Koyano, and S. Maenosono, "Chalcopyrite Nanoparticles as a Sustainable Thermoelectric Material", *Nanomaterials* 5 (4), 1820–1830 (2015).

[30] G. Gabka, R. Zybała, P. Bujak, A. Ostrowski, M. Chmielewski, W. Lisowski, J.W. Sobczak and A. Pron, "Facile Gram-Scale Synthesis of the First n-Type $CuFeS_2$ Nanocrystals for Thermoelectric Applications", *Eur. J. Inorg. Chem.* 2017 (25), 3150–3153 (2017).

[31] K. Wei, X. Zeng, T.M. Tritt, A.R. Khabibullin, L.M. Woods, and G.S. Nolas, "Structure and transport properties of dense polycrystalline Clathrate-II (K, Ba)16(Ga, Sn)136 synthesized by a new approach employing SPS", *Materials (Basel)* 9 (9), p. 732 (2016).

[32] D. Dobrynin, Y. Seepersad, M. Pekker, M. Shneider, G. Friedman, and A. Fridman, "Non-equilibrium nanosecond-pulsed plasma generation in the liquid phase (water, PDMS) without bubbles: Fast imaging, spectroscopy and leader-type model", *J. Phys. D. Appl. Phys.* 46 (10), p. 105201 (2013).

[33] E. Omurzak, T. Mashimo, S. Sulaimankulova, S. Takebe, L. Chen, Z. Abdullaeva, C. Iwamoto, Y. Oishi, H. Ihara, H. Okudera and A. Yoshiasa, "Wurtzite-type ZnS nanoparticles by pulsed electric discharge", *Nanotechnology* 22 (36), p. 365602 (2011).

[34] S. Yatsu, H. Takahashf, H. Sasaki, N. Sakaguchi, K. Ohkubo, T. Muramoto and S. Watanabe, "Fabrication of nanoparticles by electric discharge plasma in liquid", *Arch. Metall. Mater.* 58 (2), 425–429 (2013).

[35] E. Omurzak, J. Jasnakunov, N. Mairykova, A. Abdykerimova, A. Maatkasymova, S. Sulaimankulova, M. Matsuda, M. Nishida, H. Ihara and T. Mashimo, "Synthesis Method of Nanomaterials by Pulsed Plasma in Liquid", *J. Nanosci. Nanotechnol.* 7 (9), 3157–3159 (2007).

[36] L. Chen, T. Mashimo, C. Iwamoto, H. Okudera, E. Omurzak, H.S. Ganapathy, H. Ihara, J. Zhang, Z. Abdullaeva, S. Takebe and A. Yoshiasa, "Synthesis of novel $CoC_x@C$ nanoparticles", *Nanotechnology* 24 (4), p. 45602 (2013).

[37] M. A. Bratescu, N. Saito, and O. Takai, "Redox reactions in liquid plasma during iron oxide and oxide-hydroxide nanoparticles synthesis", in *Current Applied Physics* 11 (5), suppl., S30–S34 (2011).

[38] H. Doi, E. Kikuchi, S. Takagi, and S. Shikano, "Selective assimilation by deposit feeders: Experimental evidence using stable isotope ratios", *Basic Appl. Ecol.* 7 (2), 159–166 (2006).

[39] L. Chen, T. Mashimo, E. Omurzak, H. Okudera, C. Iwamoto, and A. Yoshiasa, "Pure tetragonal ZrO2 nanoparticles synthesized by pulsed plasma in liquid", *J. Phys. Chem. C* 115 (19), 9370–9375 (2011).

[40] Q. Chen, J. Li, and Y. Li, "A review of plasma-liquid interactions for nanomaterial synthesis", *J. Phys. D. Appl. Phys.* 48 (42), p. 424005 (2015).

[41] Z. Abdullaeva, E. Omurzak, C. Iwamoto, H. Ihara, H.S. Ganapathy, S. Sulaimankulova, M. Koinuma and T. Mashimo, "Pulsed plasma synthesis of iron and nickel nanoparticles coated by carbon for medical applications", *Jpn. J. Appl. Phys.* 52 (1) PART2, 1–4 (2013).

[42] L. Chen, T. Mashimo, E. Omurzak, H. Okudera, C. Iwamoto, and A. Yoshiasa, "Pure tetragonal ZrO2 nanoparticles synthesized by pulsed plasma in liquid", *J. Phys. Chem. C* 115 (19), 9370–9375 (2011).

[43] R. Zybała, M. Schmidt, P. Kamińska, M.J. Kruszewski, J. Grzonka, K. Pietrzak and Ł. Ciupiński, "Skutterudite ($CoSb_3$) thermoelectric nanomaterials fabricated by Pulse Plasma in Liquid", *Mater. Today Proc.* 5 (4), 10316–10322 (2018).

[44] G. Li, K. Kurosaki, Y. Ohishi, H. Muta, and S. Yamanaka, "Thermoelectric properties of indium-added skutterudites inx Co_4Sb_{12}", *J. Electron. Mater.* 42 (7), 1463–1468 (2013).

[45] P. Nieroda, K. Kutorasinski, J. Tobola, and K.T. Wojciechowski, "Search for Resonant-Like Impurity in Ag-Doped $CoSb_3$ Skutterudite: Theoretical and Experimental Study", *J. Electron. Mater.* 43 (6), 1681–1688 (2014).

[46] T. Caillat, A. Borshchevsky, and J.-P. Fleurial, "Properties of Single Crystalline Semiconducting $CoSb_3$", *J. Appl. Phys.* 80 (May 2013), p. 4442 (1996).

R. Zybała, M. Schmidt, K. Kaszyca, M. Chmielewski, M.J. Kruszewski, M. Jasiński, M. Rajska, and Ł. Ciupiński

[47] O. Altun, Y. E. Boke, and A. Kalemtas, "Problems for determining the thermal conductivity of TBCs by laser-flash method", *J. Achiev. Mater. Manuf. Eng*. 30 (2), 115–120 (2008).

[48] H.S. Kim, Z.M. Gibbs, Y. Tang, H. Wang, and G.J. Snyder, "Characterization of Lorenz number with Seebeck coefficient measurement", *APL Mater*. 3 (4), 1–14 (2015).

[49] E. Visnow, C.P. Heinrich, A. Schmitz, J. De Boor, P. Leidich, B. Klobes, R.P. Hermann, W.E. Müller and W. Tremel, "On the True Indium Content of In-Filled Skutterudites", *Inorg. Chem*. 54 (16), 7818–7827 (2015).

[50] L. Wang, K.F. Cai, Y.Y. Wang, H. Li, and H.F. Wang, "Thermoelectric properties of indium-filled skutterudites prepared by combining solvothermal synthesis and melting", *Appl. Phys. A Mater. Sci. Process*. 97 (4), 841–845 (2009).

[51] L. Deng, L.B. Wang, X.P. Jia, H.A. Ma, J.M. Qin, and Y.C. Wan, "Improvement of thermoelectric performance for Te-doped $CoSb_3$ by higher synthesis pressure", *J. Alloys Compd*. 602, 117–121 (2014).

[52] W. Xie, A. Weidenkaff, X. Tang, Q. Zhang, J. Poon, and T. Tritt, "Recent advances in nanostructured thermoelectric half-Heusler compounds", *Nanomaterials* 2 (4), 379–412 (2012).

[53] G. Li, K. Kurosaki, Y. Ohishi, H. Muta, and S. Yamanaka, "Thermoelectric properties of indium-added skutterudites $In_xCo_4Sb_{12}$", *J. Electron. Mater*. 42 (7), 1463–1468 (2013).